Contrib Mineral Petrol (1999) 135: 41–52

Bernardo Cesare · Cinzia Maineri

Fluid-present anatexis of metapelites at El Joyazo (SE Spain): constraints from Raman spectroscopy of graphite

Received: 14 July 1998 / Accepted: 16 November 1998

Abstract The garnet-biotite-sillimanite anatectic xenoliths in the Neogene dacite dome of El Joyazo (also called Cerro de Hoyazo, SE Spain) contain four types of graphite (I to IV), distinguished on the basis of grain size and texture. Structural characterization of graphite by Laser Raman spectroscopy (LRS) shows systematic differences in the degree of ordering among the four types: only type III is fully consistent with the granulite-facies conditions reached by the xenoliths during partial melting, the others indicate metamorphic temperatures covering amphibolite-facies conditions, with only a few examples of granulite-grade crystallinity. All graphite crystallized before or during the anatectic event, indicating that a large fraction of the graphite did not equilibrate at peak temperatures. The mm-scale coexistence of different types and degrees of ordering in the graphite suggests different origins, i.e. of biogenic derivation and "fluid-deposited", and is explained in terms of fluid-melt-graphite interaction during the anatectic event. Disequilibrium behaviour during high-temperature metamorphism and anatexis is typical of types I, II and particularly of IV, and is attributed to sluggish kinetics of solid-state graphitization, mainly owing to the limited time of the process and carbon saturation of the intergranular fluid. The coexisting, well-ordered type III graphite is the product of melting in the presence of a graphite-saturated fluid, a process that would account for the deposition of new graphite. The LRS results, together with petrologic observations, suggest that it is possible that high melt fractions can be generated by fluid-present melting of a metasedimentary protolith also in a closed system. Although this contradicts the commonly accepted hypothesis that, due to limited rock porosities, extensive fluid-present melting is precluded unless infiltration occurs, it is a possible end-member model in anatectic settings characterized by rapid heating rates and low-grade source rocks.

B. Cesare (✉)
Dipartimento di Mineralogia e Petrologia, Università di Padova, Corso Garibaldi, 37, I-35137 Padova, Italy
E-mail: bernardo@dmp.unipd.it

C. Maineri
CNR-Centro Studio Minerogenesi e Geochimica Applicata
Via La Pira, 4, I-50121 Firenze
E-mail: cmaineri@steno.geo.unifi.it

Editorial responsibility: J. Touret

Introduction

Poorly ordered, carbonaceous material (CM) of biogenic origin is widespread in sedimentary rocks, in particular rocks of pelitic composition. During prograde metamorphism, CM can be oxidized and eliminated from the rock or progressively transformed into partially to highly ordered carbon (graphite) by graphitization. Graphitization increases the degree of crystallinity of CM in a way that can be monitored by Laser Raman spectroscopy (LRS). Graphite interacts with fluids present in the rock. These fluids can be either externally derived or the products of devolatilization of the rock itself. In the case of metapelites, the most important fluid species is H_2O, released by dehydration of crystalline hydrates at low to moderate metamorphic grade (e.g. clays, micas, chlorite). At appropriate temperature and with excess graphite, this H_2O reacts to form a graphite-saturated fluid in the C-O-H system ("GCOH", Connolly and Cesare, 1993; Cesare 1995). The presence of a GCOH fluid affects the *P-T* locations of metamorphic dehydration equilibria and also has relevance for the partial melting process, since anatectic melts may dissolve relatively large concentrations of volatile components, and show marked differential partitioning of C-O-H species. As a consequence, it should be expected that graphite will behave differently in the two main types of anatexis: fluid-present melting and fluid-absent melting.

In this paper a natural example of anatexis of graphitic metapelites is studied: the xenoliths of El Joyazo. These rocks show evidence of extensive anatexis and preserve, quenched by rapid ascent and cooling, all the

textural, compositional and mineralogical features of the rocks at the time they were partially molten at mid-crustal depth. The abundance of graphite, occurring in different textural settings within the xenoliths, makes it possible to use LRS to characterize different generations of graphite within a single sample. The LRS results indicate that although all graphite crystallized before or during partial melting, only part of it is structurally equilibrated at the peak temperatures. This evidence addresses two main questions:

1. Why is disequilibrium observed only in some types of graphite?
2. What is the cause of this disequilibrium?

We answer these questions by combining knowledge of fluid-melt-rock interaction during anatexis of metapelites with information about the crystallinity of graphite. In addition, this knowledge is used to understand the mechanism of partial melting of the xenoliths.

Partial melting of graphitic rocks: theoretical approach

An important consequence of the presence of graphite in rocks undergoing anatexis has been recognized in the effect of lowering of a_{H_2O} in the fluid phase, and thus in the shift of fluid-present melting equilibria to higher temperatures (e.g. Fyfe et al. 1978). It is well known, in fact, that melting can occur both in the presence and absence of a free fluid phase (e.g. Eggler 1973; Grant 1985): the latter mechanism is also called "dehydration melting" after Thompson (1982). Due to the low porosity of high-grade rocks undergoing anatexis, and the partitioning of H_2O into the first melt produced (Burnham 1967), melting at very high metamorphic grade is commonly considered to begin or to evolve rapidly towards fluid-absent conditions (Clemens 1984; Vielzeuf and Holloway 1988).

The presence of graphite in metapelites undergoing anatexis induces other important differences, related to the melting mechanism, as briefly oultlined below. The assumptions are: (1) that the system is closed, (2) that the fluid in the rock is internally produced by dehydration, (3) that redox reactions do not take place; (4) that the amount of graphite is enough to saturate the fluid. Under these assumptions, that correspond to the condition $X_O = 1/3$ of Connolly (1995), the f_{O_2} of the system is internally imposed (Connolly and Cesare 1993). For the sake of clarity, a distinction is made between "fluid" and "melt" in the text: the former term refers to a volatile-rich phase, generally in the C-O-H system; the latter indicates a silicate-bearing liquid, in the present case of broadly granitic composition and observed as glass in natural rocks or experiments.

Fluid-absent melting

In natural metapelites the process can be simplified as a peritectic reaction of the form:

$$A = B + M \quad (1),$$

where A and B are mineral assemblages (A comprising an H_2O-bearing silicate phase and graphite), and M is an H_2O-undersaturated granitic melt. In this scenario a free fluid phase is never present to react with graphite. As the solubility of carbon in the melt is negligible, graphite essentially behaves as a refractory phase not involved in the process. This means that it will neither dissolve nor precipitate during the melting reaction, so that the net mass-balance for graphite will not vary. Graphite is only likely to recrystallize, by coarsening in the solid state, as a response to the high temperature. The foregoing conclusions are valid only under the assumption that no redox reactions occur. The effects of the presence of Fe^{3+} during the melting of a silicate/oxide system have been studied by Holloway et al. (1992), who show that graphite is not inert and quantify the consequences.

Fluid-present melting

In a graphitic system, the devolatilization of hydrous silicates produces a GCOH fluid: a mixture of H_2O, CO_2 and CH_4 with minor amounts of CO and H_2 (Ohmoto and Kerrick 1977; Holloway 1987; Connolly and Cesare 1993). Given the assumptions above (i.e. $X_O = 1/3$) this fluid will contain CO_2 and CH_4 in equal amounts: for typical mid-crustal conditions (800 °C, 6 kbar) it is H_2O-rich ($X_{H_2O} = 0.8$). Provided the fluids have not escaped the system before melting occurs, the behaviour and evolution of the fluid-melt system can be described in a triangular plot (Fig. 1): because the solubility of CO_2 and CH_4 in granitic melts is negligibly small (Holloway 1976; Clemens 1993), essentially only H_2O would be removed by the melt. This effect would move the bulk composition of the fluid within the region above the graphite saturation surface. As this is a two-phase field (GCOH fluid plus graphite) the fluid must respeciate by formation of graphite and H_2O according to a reaction similar to:

$$CH_4 + CO_2 = 2C\,(\text{graphite}) + 2H_2O \quad (2),$$

This process continues until one reactant is consumed in reaction (2). Since we are modelling $X_O = 1/3$ GCOH fluids, the entire fluid can be exhausted this way, with production of new graphite in the rock.

Thus, the partial melting reaction is expressed as:

$$A + GCOH = B + M + \text{graphite} \quad (3).$$

It follows that the two different melting mechanisms not only involve the presence or absence of a fluid phase, but also imply a very different behaviour of graphite: in both cases graphite can occur as a restitic phase. However, while it may be refractory in fluid-absent melting, it may be produced in the fluid-present scenario.

Graphitization and Raman spectroscopy

It is widely accepted that most graphite in crustal rocks represents primary organic matter graphitized under

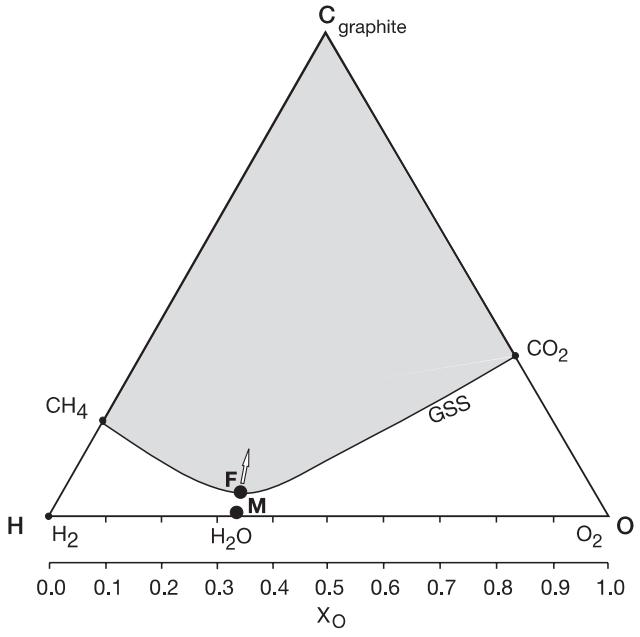

Fig. 1 Schematic C-O-H projection illustrating relationships among coexisting fluid (*F*) and melt (*M*) at 800 °C and 6 kbar. $X_O = [O/(O + H)]$ (Connolly, 1995). *GSS* is the graphite saturation surface, that delimits the single-phase field of graphite-undersaturated C-O-H fluids (*below*) from the two-phase field of graphite + GCOH (*shaded*). Fluid composition is drawn with the assumption $X_O = 1/3$ (see text for details). The *arrrow* indicates the effect of selective H_2O fractionation into the melt

high-temperature conditions (e.g. Buseck and Huang 1985), and that in metasedimentary rocks the process of graphitization proceeds through the transition of CM in unmetamorphosed or low-grade to graphite in medium- to high-grade metamorphic rocks (French 1964; Grew 1974; Itaya 1981).

During the process of graphitization, both chemical and structural changes take place in the organic material. Chemical maturation involves essentially the expulsion of H, O, and N from the crystallite structure (Grew 1974; Itaya 1981; Wedeking and Hayes 1983), while structural reorganization proceeds both within hexagonal aromatic planes and perpendicularly to them. The physical aspect of the process is characterized by the increase of in-plane (001) diameter (La, Fig. 2) and of stacking height (Lc) (Oberlin et al. 1980; Beny Bassez and Rouzaud 1985), and by the reduction of interplanar

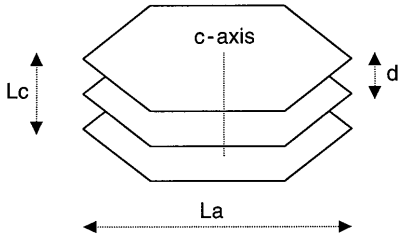

Fig. 2 The structure of well-ordered graphite (crystal symmetry $P6_3/mmc$, space group D^4_{6h}). (Crystallinity parameters: *Lc* mean stacking height, *La* mean basal diameter, *d* interplanar distance)

values (d) of graphite crystallites. The values of these parameters define the degree of crystallinity of CM (Tuinstra and Koenig 1970), basically reflecting the structural ordering of C atoms in the crystal lattice. The process of graphitization, and therefore the degree of crystallinity, are mainly controlled by temperature, and to a lesser extent by pressure, shear strain (Ross and Bustin 1990), time, catalytic agents in the CM matrix, and type of organic precursor (Landis 1971; Grew 1974; Pasteris and Wopenka 1991). The degree of crystallinity of CM is then considered as sensitive to and, in many cases, the unique indicator of the metamorphic grade of its host rocks. Furthermore, given the irreversibility of the graphitization process, the highest degree of CM structural ordering reached in a prograde metamorphic event will generally be retained during subsequent retrogressive events (Pasteris and Wopenka 1991). The degree of crystallinity of graphite can be inferred by means of different analytical techniques (discussed by Wopenka and Pasteris, 1993), among which LRS, XRD (X-ray diffraction) and HRTEM (high resolution transmission electron microscopy) are the most commonly applied in petrology.

The Raman spectrum of CM

The Raman spectrum of carbonaceous material consists of two distinct spectral regions: the first lies between 1200 and 1700 cm^{-1} and the second between 2300 and 3300 cm^{-1} (Tuinstra and Koenig 1970). They are usually referred to as "first-" and "second-order spectrum", respectively. The theoretical models of Raman scattering of graphite have been treated in a number of publications quoted in Wopenka and Pasteris (1993) and Yui et al. (1996). For the purpose of this work it will suffice to recall the main aspects concerning the origin and interpretation of Raman bands of CM. For well-crystallized CM ("graphite"), the first-order spectrum shows a single peak at ca 1582 cm^{-1}, usually referred to as the "ordered (O) peak", which is attributed to the within-sheet vibration mode (E_{2g2}) of graphite with D^4_{6h} crystal symmetry (Tuinstra and Koenig 1970). For less-ordered CM a second peak appears in the first-order spectrum at ca 1355 cm^{-1}, which is attributed to a disorder-induced Raman mode (Nemanich and Solin 1979). The "O" and "D" Raman bands are the most intense in the first-order spectrum of CM. One additional small band may also occur around 1622 cm^{-1}, which, similarly to the "D" peak, results from a decrease in crystallite size with decreasing structural order (Nemanich and Solin 1979). The second-order spectrum of well-ordered graphite is characterized by three bands that are essentially due to both combination and overtone scattering modes (Nemanich and Solin 1979) and occur at relative frequencies of ca 2450 cm^{-1}, ca 2735 cm^{-1} ("S"-peak), and ca 3248 cm^{-1}. As can be observed in Wopenka and Pasteris (1993, Fig. 1) the "S" peak of well-ordered graphite appears as a doublet

whereas, for less-ordered CM, it becomes broader. A further band at 2950 cm^{-1} is sometimes reported in the second-order spectrum; possibly related either to the disorder-induced mode theoretically predicted by scattering models, or to the C-H stretching modes of non-carbon atoms present as impurities in the structure (Tsu et al. 1978).

Since the degree of crystallinity is mainly temperature dependent, a correlation between the relative D and O peak intensities and formation temperature has long been suggested (e.g. Michel-Levy and Lautie 1981). However, it is only more recently that systematic studies of variably ordered forms of CM indicate a clear relationship between their Raman features and genetic conditions. Pasteris and Wopenka (1991) and Wopenka and Pasteris (1993) presented a systematic study of Raman properties of CM hosted by metapelites ranging from greenschist to granulite facies. Their results stress the applicability of LRS to natural occurrences of graphite and demonstrate that Raman spectra can provide a quantitative model of CM structural ordering: position, intensity and average widths of Raman bands, as well as the ratios of both peak intensities and areas are the most important parameters. After these studies LRS has become a complementary, reliable tool in providing fast, non-destructive microanalysis of variably ordered forms of CM of geological interest. According to Wopenka and Pasteris (1993), after instrument calibration, the reliability of CM Raman features is so good that, especially for a specific suite of host rocks, the degree of ordering could well be inferred even by visual estimates of the first-order spectrum. In this case, inverse correlation between intensity of D peak and degree of crystallinity makes it possible to infer the metamorphic grade of host rock.

Compared to other techniques, a major advantage of LRS is the possibility of collecting spectra from in situ single graphite samples, which thus retain their original textural relationship within the host rock. This peculiar feature makes LRS a method well suited for texturally complex rocks, such as El Joyazo graphitic xenoliths. These rocks are ideal for the application of this technique because all graphite populations under examination are not only hosted by the same lithotype, but also occur in the same microsample. This fact, besides minimizing matrix effects that may influence the Raman signal, also permits comparison with the results obtained on the four metamorphic categories (A–D) recognized in graphitic metapelites by Wopenka and Pasteris (1993).

Metapelitic xenoliths of El Joyazo

Geo-petrographic setting

The small dacitic lava dome of El Joyazo (also called Cerro de Hoyazo) is part of the Neogene volcanic province of the Betic Zone (SE Spain). In this area, the calc-alkaline to shoshonitic activity is dated at 6.5–8.5 Ma (Lopez Ruiz and Rodriguez Badiola 1980) and is a result of the lithospheric thinning and upwelling of the upper mantle during the opening of the Alboran Sea (De Larouziere et al. 1988). The dacite of El Joyazo is interpreted as the contaminated product of crustal anatexis (Zeck 1968, 1970; Munskgaard 1984, 1985). This interpretation is supported by the occurrence of abundant crustal enclaves with evidence of partial melting.

As described by Zeck (1968), the most abundant enclaves in the dacite consist of garnet-biotite-sillimanite xenoliths. These xenoliths constitute roughly 1% in volume of the lava, reaching up to 60 cm in diameter. They are interpreted as restites from metapelitic protoliths, formed after extraction of a large amount (30–60 wt%) of granitic melt (Cesare et al. 1997). Partial melting of the xenoliths occurred at about 5–7 kbar and 850 ± 50 °C, affecting a metasedimentary complex comparable to that cropping out in the adjacent Betic Cordillera.

The main petrographic and chemical features of the xenoliths are reported by Cesare et al. (1997). They are well foliated and contain biotite (Bt), plagioclase (Pl), fibrolitic sillimanite (Sil), garnet (Grt), silicate melt (glass), graphite, apatite. Additional phases may include ilmenite (Ilm), hercynite (Her) and cordierite (Crd). Quartz (Qtz) is present only as minute inclusions in plagioclase or garnet, K-feldspar (Kfs) is absent and biotite makes up about 40% of the rocks. The average grain size in the biotite-sillimanite matrix of the xenoliths is about 1 mm, but garnet and plagioclase are up to 1 cm across. Cordierite, where present, forms poikiloblasts of several centimetres in size. Graphite is abundant throughout the rocks (Fig. 3a) as both inclusions in minerals and flakes defining the foliation with biotite. Rhyolitic glass is present as primary melt inclusions in all minerals and as thin layers and patches along the foliation.

Fig. 3a–f Photomicrographs illustrating graphite types and textures. **a** General view of graphite abundance and mode of occurrence in the xenoliths of El Joyazo. Graphite (*bright*) types I (arrows) II and III can be recognized (see text and following photomicrographs). Reflected light (RL), crossed polars (XPL), *width* of view = 15 mm. **b** Coarse lamellae of type I graphite (*black*) aligned along biotite-plagioclase boundaries. Types II (stars) and III (arrows) are also shown. Transmitted light (TL), plane-polarized light (PPL), *width* of view = 0.3 mm. **c** Type I graphite within a fibrolite-glass aggregate. RL, PPL, *width* of view = 0.3 mm. **d** Coarse lamellae of type I graphite (*bright*) at the periphery of a fibrolite-glass aggregate (*upper-right corner*). The *dark* part of photomicrograph is a crystal of biotite containing minute lamellae (*arrows*) of type IV graphite. RL, XPL, *width* of view = 0.25 mm. **e** A crystal of plagioclase rich in type III graphite inclusions, associated with melt inclusions. TL, PPL, *width* of view = 0.25 mm. **f** Type III graphite associated with melt inclusions in a crystal of plagioclase. Graphite is a solid inclusion, as demonstrated by the relationships between inclusion walls and graphite (*arrows*) TL, PPL, *width* of view = 0.15 mm

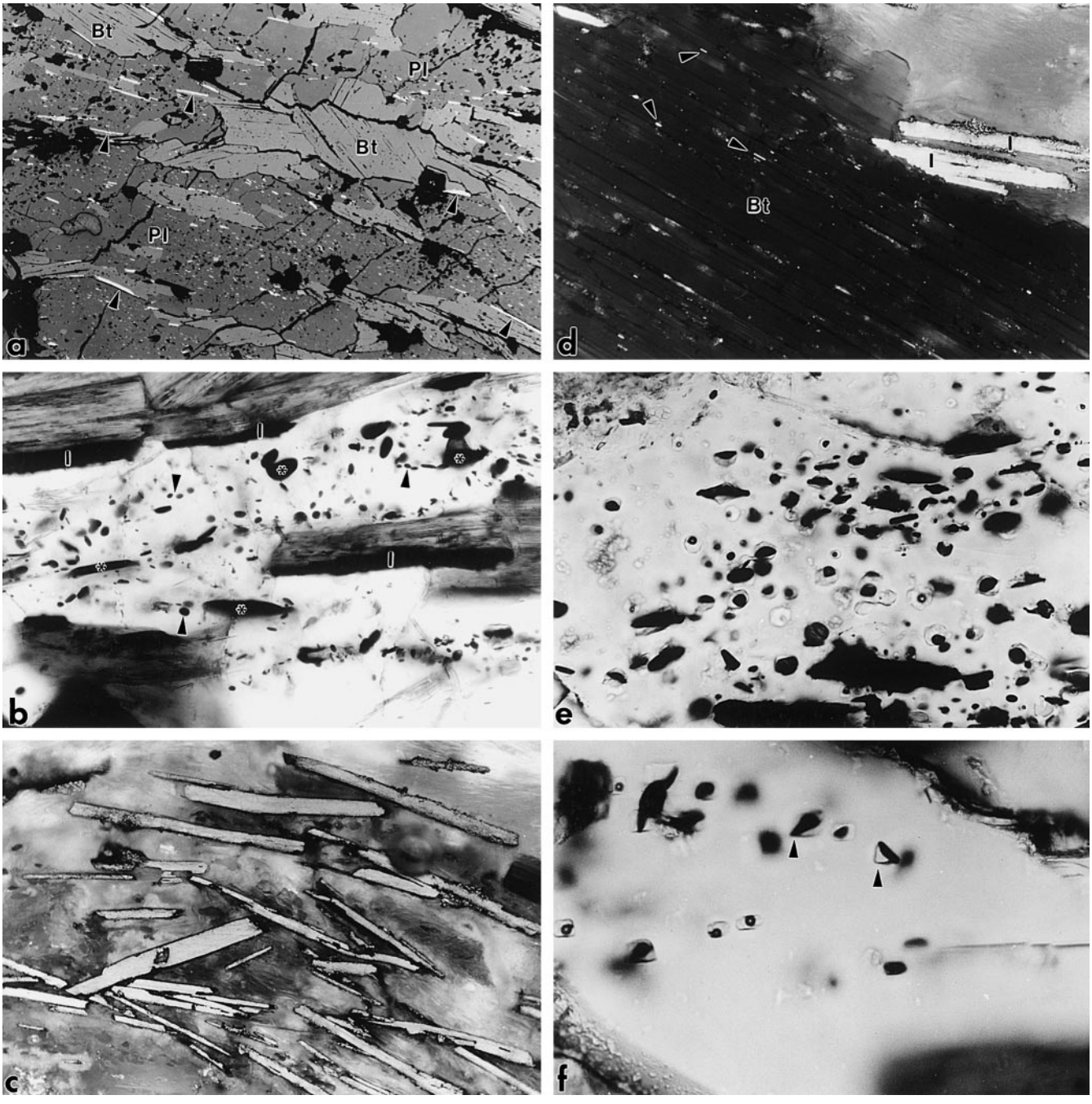

Melt and fluid inclusions

Despite the abundance of melt inclusions, the xenoliths are virtually free of fluid inclusions. Two-phase (vapour + glass) inclusions, ranging from < 5 to 100 μm in size, occur in all mineral phases except sillimanite. Melt inclusions exhibit regular, negative-crystal shapes, with a constant vapour/glass ratio of about 0.2. As outlined by Cesare et al. (1997), their textural position within host phases is compatible with a primary trapping (Roedder 1984). Glass is transparent, showing no evidence for divitrification or recrystallization. The bubbles are essentially empty, shrinkage bubbles, with no detectable Raman-active components, except in rare cases, in which a strong fluorescent band in the region of C-H stretching modes (2600–3000 cm^{-1}) was observed.

Graphite textures

The xenoliths contain more than 1 wt% graphite, which occurs in several textural settings, so that different types can be recognized and described in order of their abundance.

Type I

These are coarse flakes (up to 150 μm in long dimension), generally aligned within biotite-rich layers (Fig. 3b), or at the periphery of fibrolite-melt nodules (Fig. 3c and d). This type of graphite is rarely deformed, and appears as well-crystallized, homogeneous lamellae. In rare instances, in particular where associated with fibrolite, lamellae seem to be composed of aggregates of coalescent smaller crystals.

Type II

These coarse flakes (up to 100 μm) occur as inclusions, mainly in plagioclase and biotite, and not associated with melt inclusions (Fig. 2b).

Type III

These are fine lamellae (< 20 μm), often associated with melt inclusions (< 50 μm), present in all minerals except fibrolite. This type of graphite is particularly abundant in plagioclase and biotite, giving the host phase a "turbid" appearance, owing to the abundance of minute (< 5 μm) melt and graphite inclusions (Fig. 3b and e). Graphite and melt inclusions do not always occur together and, in the same host crystal, they may be isolated from each other. In this case, the isolated graphite can be both of type II (coarse grained) and type III (fine grained). Due to such lack of systematic association, and because of the textural relationships of graphite lamellae to the walls of melt inclusions (Fig. 3f), the graphite is interpreted as solid inclusions; it cannot be a daughter mineral precipitated from the cooling melt. This implies that type III graphite was formed (along with type II) before the growth of the host mineral and entrapment of melt inclusions. It is likely that graphite flakes acted as preferential sites for the entrapment of melt inclusions, by creating imperfections at the surfaces of host minerals (Roedder 1984).

Type IV

This type consists of very fine grained lamellae (< 2 μm) in biotite (Fig. 3c) and plagioclase. Type IV is not associated with melt inclusions and may represent relict graphite from the metasedimentary protolith.

From visual estimates, types I and II account for about 60 vol.% of the total graphite, the remainder being made of type III, with type IV present only in negligible amounts.

For the sake of completeness, LRS analysis was also done on the CM of the phyllites envisaged as the possible protoliths of the xenoliths (Cesare et al. 1997). These rocks contain two textural generations of graphite, defined as *type V* (< 2 μm, very abundant) and *type VI* (up to 40 μm, rare).

Raman spectroscopy of graphite

Analytical technique

The degree of crystallinity of graphite in the xenoliths was analysed in ten polished sections, where the different types could easily be recognized.

The LRS analyses were carried out at Centro Studio Minerogenesi e Geochimica Applicata of Italian Research Council (CNR) in Firenze, using a Jobin-Yvon S 3000 triple spectrograph, equipped with a Spectra-Physics continuous Ar-ion laser source, an Astromed Ltd. N_2-cooled CCD detector and an Olympus BH-2 optical microscope.

The El Joyazo graphites do not permit, as suggested in Pasteris and Wopenka (1991), focussing of the laser beam onto grains that lie below a transparent phase (e.g. silicate) to avoid collection of data from surfaces disrupted by polishing. Such a technique could produce spectra indicating a lower degree of crystallinity than the grains actually have. As clearly shown in Fig. 3a–f, except when inside melt inclusions, our graphites are always exposed at the surfaces of polished sections. Therefore, in the present work, the laser beam was focussed onto (apparently) undamaged sample surfaces, using both the 514.5 and the 488 nm lines, with variable laser power of < 5 to 20 mW. Entrance (S_1) and exit (S_3) slits were set at 200 μm; the spectral resolution was ca 5 cm^{-1}. The objectives used were 50x or 100x, investigating the spectral regions 1000–1750 cm^{-1} and 2350–3350 cm^{-1}. Integration times were between 10 and 20 seconds for each acquisition. To enhance the signal-to-noise ratio, the final spectrum was obtained by summing 5 spectra acquired under the same operating conditions. The spectra were then processed by means of the Jobin-Yvon "PRISM 3.1" software. Due to the lack of appropriate graphite standards, analyses of representative graphite types were duplicated with the Dilor Microdil 28 Raman spectrometer at the Vrije Universiteit of Amsterdam (see Burke and Lustenhower 1987, for instrumental detail).

Results

The results of LRS analyses on the graphitic xenoliths are summarized in Table 1 and Fig. 4, and compared with the metamorphic categories defined by Wopenka and Pasteris (1993). The large lamellae of *type I* graphite show a large variation in spectral parameters, representing variable degrees of structural ordering. As shown in Table 1, most of the spectra can be compared to the intermediate B and C categories (e.g. Bt and Grt zones and St (staurolite), Ky (kyanite) and And (andalusite) zones, respectively) of Wopenka and Pasteris (1993), although all metamorphic categories, ranging from chlorite to sillimanite grade, are represented. It appears that this intermediate degree of crystallinity, generally providing spectra similar to those reported in Fig. 4-1 and 4-2, actually characterizes both deformed and undeformed graphite flakes, as well as single crystals and large polycrystalline aggregates. The spectra were obtained in both basal and perpendicular to (001) crystal sections, but no appreciable orientation effects were observed. Multiple spot analyses on different areas of the same graphite crystal provided similar spectra, within the same metamorphic category, so that type I graphite can be considered spectroscopically homogeneous at single grain/aggregate scale. Such homogeneity at laser beam scale is in agreement with the observations

Table 1 Raman spectral parameters for representative graphites in the xenoliths of El Joyazo (*n.a.* not applicable, *(n)* number of spectra, *w* peak widths calculated at half height, *1*, 2*, 3*,4** spectra reported in Fig. 4)

Graphite type		Sample	Peak position (Rcm^{-1})			D_w	O_w	D/O	D/O	Metamorphic grade
			D	O	S	(cm^{-1})	(cm^{-1})	intensity	area	Metapelitic host lithologies
I		HO3L XO	1358	1583	2722	21	29	0.12	0.25	Andalusite
		HO3L XT	n.a	1582	2725	17	–	0.0	0.0	Sillimanite
	1*	HO3B 19	1358	1585	2715	20	48	0.50	0.59	Chlorite/biotite
		SPE 5 1	1355	1580	2728	20	48	0.21	0.32	Subgarnet/staurolite
		SPE 5 2	1357	1581	2717	22	49	0.33	0.55	Chlorite/biotite-garnet
		SPE 5 5	1355	1583	2725	23	45	0.23	0.44	Garnet/staurolite
		HO3C 4	1352	1579	2729	22	44	0.31	0.53	" "
		HO3C 7	1359	1588	2730	21	49	0.26	0.35	Staurolite
		HO3C 8	1361	1579	2730	20	46	0.25	0.34	"
		HO3C 9	1366	1585	2736	23	40	0.21	0.25	Andalusite
		HO3C 10	1357	1580	2728	16	29	0.33	0.27	Staurolite
		HO3D 2	1351	1585	2724	17	45	0.09	0.13	Sillimanite
		HO22 D 4	1359	1581	2715	17	49	0.10	0.13	"
		HO3 D 5	1355	1587	2725	23	44	0.35	0.51	Subgarnet
		HO3 D 8	1357	1583	2712	21	40	0.30	0.27	Staurolite
		SPE 65 LA	1366	1587	2726	20	33	0.50	0.41	Chlorite/biotite
		SPE 65 L1	1580	1355	2735	16	32	0.16	0.24	Andalusite
		SPE 65 L2	1362	1580	2721	19	38	0.41	0.53	Chlorite/ biotite-garnet
II		HO3L B1	1354	1588	2722	20	48	0.21	0.32	Andalusite
		HO3L B2	1358	1580	2617	21	35	0.20	0.26	Staurolite
		SPE 5 P1	1355	1586	2715	25	43	0.31	0.50	"
	2*	SPE 5 P3	1357	1581	2728	25	50	0.25	0.41	"
		SPE 5 P 11	1360	1582	2725	19	41	0.10	0.14	Sillimanite
III ($n = 4$)	3*	SPE $5_{5–9}$	1357 ± 5	1582 ± 4	2716 ± 4	22 ± 2	≈ 46	≈ 0.10	≈ 0.18	Andalusite
($n = 10$)	4*	$HO3L_{1–10}$	n.a.	1585 ± 3	2729 ± 7	–	18 ± 2	0.0	0.0	Sillimanite
IV		HO3 R1	1357	1579	2723	23	39	0.18	0.23	Andalusite
		HO3 R5	1355	1583	2716	20	43	0.15	0.29	"
		SPE 5 R6	n.a.	1582	2728	–	19	0.0	0.0	Sillimanite
VI		HO13a 21	1360	1574	2717	38	19	0.11	0.20	Andalusite
		HO13a 23	1357	1582	2732	28	30	0.22	0.21	Staurolite

of Wopenka and Pasteris (1993) and Yui et al. (1996). Relevant features in the second-order spectrum are the relatively variable S-peak position and, in some spectra, the appearance of the 2950 ca cm^{-1} peak (Fig. 4-1). This band is only observed in some of the most disordered type I graphites, which suggests that it may be related to the presence of C—H impurities in the incompletely mature CM structure.

Compared with those of type I, Raman spectra of *type II* graphites show a more restricted variability of spectral parameters. Since biotite-hosted graphite was found to blur under the laser beam, the Raman parameters in Table 1 are mainly given relative to plagioclase-hosted type II graphites, The peak quantified parameters allow comparison with the St-And zone samples ("C" metamorphic category) of Wopenka and Pasteris (1993). Unlike type I, type II graphite does not record lower metamorphic grades. The second-order spectra of type II graphites show an unresolved S peak, whereas minor bands exhibit appreciable signal-to-noise ratios (Fig. 4-2).

Most of *type III* graphites show an intense and well-shaped O band, at a mean position of 1582 cm^{-1}, which is narrower than in any other graphite type (Fig. 4-4). Where present, the ca 1355 cm^{-1} band is small, so that the D/O ratios of intensities and areas are very close to zero (Table 1; Fig. 4-3). These features indicate a high degree of structural order for type III graphite, analogous to the D category of Wopenka and Pasteris (1993), typical of very high temperature (i.e. sillimanite zone to granulite facies). In the second-order spectrum, the S peak of this graphite type shows a well-resolved doublet (arrow in Fig. 4-4) and a small but sharp peak is observed at ca 3250 cm^{-1}.

Owing to its minute size (< 2 μm) and deterioration of host biotite, Raman analysis of *type IV* graphite was very difficult or precluded. A few good quality spectra of plagioclase-hosted type IV graphites indicate a range of crystallinity from garnet to andalusite and, in one case, sillimanite metamorphic zones (Table 1).

Analysis of minute *type V* CM from the phyllitic protolith was not successful, as for most of the larger *type VI* crystals that exhibit instability under the laser beam. However, spectra of two type VI graphites indicate, again, a rather variable degree of crystallinity, comparable with that of type IV.

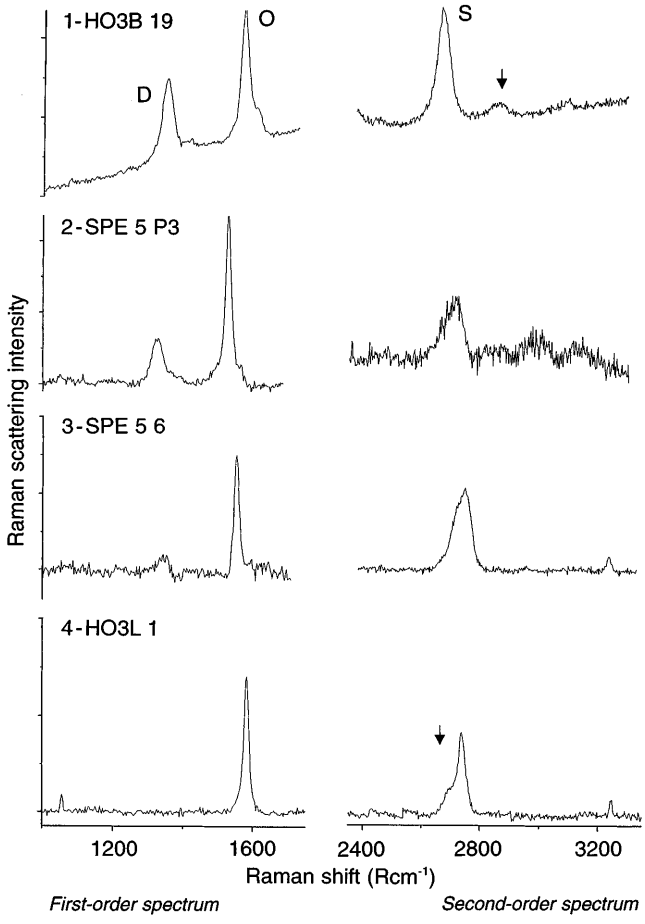

Fig. 4. 1–4 Examples of Raman spectra and metamorphic categories of El Joyazo graphites: **1** chlorite-biotite zone; **2** staurolite-andalusite zone; **3** andalusite zone; **4** sillimanite zone. *Arrows* in spectra nos. 1 and 4 indicate the ≈2950 Rcm^{-1} band, and the well-resolved S-peak doublet (≈2680^{-1} and 2735 Rcm^{-1} bands), respectively. See text for details

For some crystals of type IV, V and VI it was possible to collect visual estimates during real-time aquisition of the spectra, before deterioration. These observations indicate a rather low degree of cristallinity, similar to the spectrum in Fig. 4-1 (i.e. to the upper Chl (chlorite) to Chl/Bt metamorphic zones as in Wopenka and Pasteris, 1993). This suggests that the average degree of crystallinity of both type IV and VI graphite is lower than that indicated in Table 1, where only quantified spectra are reported.

The Raman parameters reported in Table 1 and spectrum visual estimates indicate the occurrence of variably ordered forms of graphite in the xenoliths of El Joyazo. As a whole, it appears that the largest lamellae, such as types I and II, are less ordered than type III graphite, for which the highest degree of ordering, compatible with granulite-facies metamorphism, was consistently recorded in all the analysed samples.

The instability of both type IV and VI graphites and of biotite-hosted graphites remains an unexplained, although common phenomenon. In the latter case it is clearly due to some host effect (probably related to the poor heat-sink character of biotite), whereas in the former case, Wopenka and Pasteris (1993) suggest the possibility of a positive correlation between CM degree of disorder and instability under the laser beam. If this is the case, we can speculate that the average degree of structural order of the phyllitic protolith was relatively low.

Discussion

The LRS shows that the anatectic xenoliths of El Joyazo contain graphite populations with different degrees of crystallinity, corresponding to metamorphic grades ranging from upper greenschist to granulite facies. This observation conflicts with the high temperatures experienced by the xenoliths. However, this is not the only peculiarity that emerges from investigation of the xenoliths. The occurrence of melt inclusions in all minerals indicates that all solid phases grew in the presence of melt. Even the rare, minute crystals of quartz included in garnet, possibly representing an exhausted reactant, contain melt inclusions. This paradox is examined in the following paragraphs, in the framework of a possible melting model for the xenoliths. The model is constrained by the following data and indications, in part outlined by Cesare et al. (1997):

1. Anatexis involved fine-grained graphitic metapelites, comparable, in bulk chemistry with the phyllites exposed in the adjacent Betic Cordillera, and which contain Qtz, Pl, Chl, Ms, Grt, Bt, Ilm and graphite.
2. The H_2O content is 3–4 wt% in the phyllite and 1–2% in the xenoliths, whereas the graphite content is respectively 0.5% and 1.0% (determined by C-H elemental analyser);
3. The H_2O content of the glass in the xenoliths (semiquantitatively deduced by EMPA closure values) ranges from 4.5 to 6.0 wt%, well below the values of H_2O saturation for rhyolitic melts at 5–7 kbar (10–13 wt%, Holtz et al. 1995).

Within-sample variations of Raman spectra

The occurrence of different degrees of crystallinity cannot be the result of processes developing after the anatexis, as all graphite generations were present before and during entrapment of melt inclusions, and are not associated with fluid inclusions. Hence, models for graphite precipitation by interaction between fluids and cooling melts (e.g. Stevens 1997) are inapplicable in the present context. Since the xenoliths appear to have been rapidly exhumed and quenched after mineral equilibration at high temperature (850 ± 50 °C; Cesare et al. 1997), it follows that only part of the graphite equilibrated at the conditions of partial melting. Such disequilibrium occurs at the thin-section scale, i.e. over a distance of less than 1 cm; similar behaviour has been reported in the literature (e.g. Wopenka et al. 1988), and

attributed to coexistence of graphites of different origins (Wopenka and Pasteris, 1993).

The degree of crystallinity of graphite from El Joyazo xenoliths is not related to the grain size of graphite lamellae. In fact it is highest in type III, which is fine grained but not as fine as type IV. On the other hand, the poorest ordering is observed in both the smallest (type IV) and largest crystals (types I and II). Such evidence is difficult to reconcile with a graphitization process accompanied by grain size coarsening during progressive heating, in which the degree of crystallinity should be directly proportional to grain size. Solid-state graphitization is the main process to be expected during fluid-absent melting of Fe^{3+}-free graphitic metapelites, because graphite does not interact with the anatectic melt and does not form as a product of the melting reaction. On the other hand, fluid-present melting allows the coexistence of at least two types of graphite: the primary carbonaceous material of the metasediment and a new graphite, formed at the onset of anatexis by reaction (3). Such new graphite can be identified as "fluid-deposited" according to the terminology of Wopenka and Pasteris (1993). Where formed at high metamorphic grade (e.g. Hollister 1980; Katz 1987) this type of graphite provides highly ordered Raman spectra, compatible with its inferred genetic conditions.

In the xenoliths, the highest ordering is typical of type III graphite. All the other types, though some crystals may be highly ordered, generally show lower degrees of crystallinity. We propose that the most plausible origin for type III graphite is through deposition by saturation of a C-O-H fluid phase. Since type III graphite is generally associated with melt inclusions, it is likely to have formed during melt-fluid interaction, namely during fluid-present melting. Owing to its fluid-deposited origin, it differs from the other types, and represents the only graphite that newly crystallized, and therefore acquired a high structural order. This explains why it is the only generation of graphite fully equilibrated at the *P-T* conditions of anatexis. The mechanism proposed for formation of type III graphite does not coincide exactly with that defined as "fluid deposition" by Wopenka and Pasteris (1993) and Pasteris and Chou (1998). This is because, in the present case, graphite precipitated by interactions between two "solutions", a GCOH fluid and a silicate melt. If the GCOH fluid is at $X_O = 1/3$ and the melt remains undersaturated, reaction (2) can lead to the complete exhaustion of the volatile phase. Conversely, for the condition $X_O = 1/3$ a CO_2- or CH_4-rich residual fluid should form (Cesare 1995), with the possibility of entrapment of fluid inclusions. As both melt inclusions and interstitial glass are clearly H_2O-undersaturated, and because no fluid inclusions have been observed, we believe that the assumption of $X_O \neq 1/3$, is a good first approximation model for this system. As noted above, such a condition can be attained, in the case of internal derivation of the fluid, by subsolidus devolatilization of crystalline hydrates and retention of the fluid in the system.

The graphite crystals with lower degrees of crystallinity are unlikely to represent the products of high-temperature fluid deposition, and are better modelled by "solid-state" transition processes. Concerning the lack of equilibration of some crystals of the other graphite types, a possible cause can be sought among the factors controlling graphitization. The duration of the thermal event and the composition of fluids seem to have been the most important factors in determining the behaviour of the xenoliths. In particular, limited time and carbon saturation of the fluid are factors that inhibit or slow down the kinetics of ordering, allowing preservation of relatively disordered graphite crystals at high temperatures (Large et al. 1994). Carbon saturation of the fluid was certainly attained during prograde heating and anatexis, as demonstrated by the abundance of graphite in the xenoliths and inferred protoliths. The limited time, through a very fast heating rate and subsequent rapid exhumation by eruption, is difficult to quantify. However available data on the thermal and geochronological evolution of the area (Platt et al. 1996; Zeck 1996) suggest that the crust now exposed in the Betic Cordillera experienced rapid extension, accompanied by a transient thermal pulse and by underplating of mantle-derived basic magmas. This was the cause of a rapid, almost isobaric heating, similar to a contact metamorphic regime (Houseman and England 1986; Platt and England 1994; Bertotti et al. 1997). This extensional evolution and the associated volcanism seem to have occurred over a very short time interval of a few million years during the Miocene (Zeck et al. 1992; Platt et al. 1996 and references therein).

Inhibition of graphitization by the above factors may explain why all graphite types, except III, contain evidence for various stages of incomplete re-equilibration of the metasedimentary graphitic material. This is consistent with the evidence that the degree of ordering of these types is equal to or higher than that of the suggested phyllitic protolith. From the textural point of view, the protolith contained two types of graphite, both fine- and coarse-grained. Similar populations are observed in the xenoliths, with the occurrence of coarse types I and II side by side with fine-grained type IV. Variations of degree of ordering among types I, II and IV are probably related to differences in secondary factors, such as primary grain size, efficiency of wetting by intergranular fluid or melt, textural position and inclusion by host minerals.

Fluid-present versus fluid-absent melting: the role of disequilibrium and graphite

Because type III graphite is fine grained and commonly associated with melt inclusions, we have interpreted it as the result of graphite deposition during partial melting by reaction (3). Thus, type III graphite represents evidence for the occurrence of fluid-present partial melting in the formation of the xenoliths of El Joyazo.

Fluid-present melting is generally considered to characterize the initial stages of anatexis and, due to the usually low availability of free H_2O in high-grade rocks, regarded as unable to produce large amounts of H_2O-saturated melt (only a few percent). The large melt fractions (30–60 wt%) estimated in the xenoliths, and their markedly H_2O-undersaturated character, are more typical of fluid-absent melting (e.g. Vielzeuf and Holloway 1988). However, as shown above, a fluid-absent melting model is difficult to apply to the present study.

Since primary melt inclusions are trapped during growth of the host mineral (Roedder 1984), it follows that in the xenoliths biotite, garnet and plagioclase crystallized (or recrystallized) in the presence of melt, i.e. during anatexis. Acicular sillimanite is too fine grained to trap melt inclusions, but is so intimately intergrown with interstitial glass (Fig. 3 of Cesare et al. 1997) that it is also likely to have grown in the presence of a melt. The assemblage Pl-Bt-Grt-Sil-melt is typical for the *P-T* conditions estimated in the xenoliths (i.e. Le Breton and Thompson 1988); and the abundance of biotite at temperatures in excess of 850 °C can be explained by both its high Ti content (Patino Douce and Johnston 1991) and the lack of quartz as a restite phase. However, consider the most common melting reaction observed at these *P-T* conditions (e.g. Vielzeuf and Holloway 1988):

$$\text{Bt} + \text{Pl} + \text{Qtz} + \text{Sil}\ (\pm\,\text{fluid}) = \text{Grt} + \text{melt}\ (\pm\,\text{Kfs}) \qquad (4)$$

Regardless of the role of fluid and K-feldspar, this mechanism of partial melting accounts for the presence of melt inclusions only in garnet, because all the other solid phases are consumed. Since there are no melting reactions simultaneously producing the assemblage Bt-Grt-Pl-Sil-melt, the equilibrium progress of any peritectic reaction cannot be applied to the present study, as it would result in the presence of mineral phases (the reactants) free of melt inclusions. The most likely mechanism by which all restite phases may crystallize at the same time that melt is formed is by rapid, disequilibrium melting provided that the starting assemblage has not readily equilibrated during prograde metamorphism. Disequilibrium behaviour is favoured in natural environments characterized by high heating rates (e.g. in contact metamorphism and in some extensional basins). This situation can be compared to melting experiments in which anatexis is modelled on certain synthetic compositions (e.g. Vielzeuf and Montel 1994) or natural low-grade rocks. As the *P-T* values of interest are reached in a few minutes, the bulk composition is allowed to equilibrate only at such conditions, by-passing the intermediate stages. In this case the reacting solid assemblage does not contain (or contains only in minor amounts) the minerals stable in the field of anatexis, and all restite crystals (or most of them) will grow during partial melting. From this point of view the term disequilibrium essentially refers to the presence of the reactant assemblage outside its stability field. In fact the reaction products appear equilibrated from both mineralogical and chemical point of views. This model seems to be applicable to the actively expanding basin in which the xenoliths of El Joyazo occur (Platt et al. 1996). Considering that the protolith was probably a low-grade phyllite (see above), it is possible that most reactions typical of amphibolite-facies conditions were by-passed or overstepped, until melting occurred via a disequilibrium reaction similar to:

$$\text{Chl} + \text{Ms} + \text{Qtz} + \text{Ilm} + \text{GCOH fluid} = \text{Grt} + \text{Pl} + \text{Sil} + \text{Bt} + \text{melt} + \text{graphite} \qquad (5).$$

In this way chlorite, muscovite, quartz and ilmenite (and possibly staurolite, K-feldspar and kyanite) were consumed. As long as their amounts were small compared to those in the restite, this process also allows for the presence of some plagioclase, biotite, garnet and fibrolite in the rocks before melting.

The disequilibrium melting of the xenoliths can further be investigated by analysing the effect of the presence of a graphite-saturated fluid, in which X_{H_2O} is about 0.80 (Connolly and Cesare 1993). The resultant lowering of ^aH_2O in the fluid has the effect of displacing devolatilization and fluid-present melting equilibria towards lower and higher temperatures, respectively (e.g. Kerrick 1972). In a system undergoing heating at a given *P*, this favours devolatilization and delays melting. The temperature interval over which the rock can release H_2O by subsolidus dehydration becomes substantially larger. This may account for the production of the H_2O necessary for the fluid-present melting behaviour assumed on the basis of graphite crystallinity. Furthermore, reduction of ^aH_2O has the effect of diminishing the H_2O solubility and H_2O content of the melt, so that higher melt fractions can be obtained at a given bulk H_2O content (Clemens and Vielzeuf 1987). From the data of Johannes and Holtz (1996), melts generated at equilibrium in this way should contain less than 10 wt% H_2O, but significant overstepping (e.g. 50 °C) could decrease this amount to less than 7%. These are H_2O contents of haplogranitic melts, which are considered a good model for the melting of natural pelites, as long as Ca, Fe and Mg occur in relatively small amounts in the melt (Vielzeuf and Montel 1994). The estimated H_2O contents of the melt in the xenoliths are higher than the minimum amount (Holtz et al. 1992) predicted for fluid-absent melting at the estimated *P-T* conditions of the xenoliths. This may be a further evidence of the fluid-present character of the melting process.

Concerning the fluid budget involved in the model process, the available chemical data on xenoliths, phyllites and melt show that: (1) the initial H_2O content of the phyllite can account for production of 50 wt% melt plus a restitic xenolith; (2) the amount of H_2O consumed by such a melt could form, by progress of reaction (3), up to 0.45 wt% of fluid-deposited, type III graphite, i.e. more than half of the graphite in the primary phyllite. Thus, the proposed model can consistently explain the amounts of both melt produced and graphite precipi-

tated by partial melting in the presence of an internally derived fluid, in a closed-system environment. However, it has one major drawback in the high porosity required. As discussed by Clemens and Vielzeuf (1987), the porosity of high-grade metamorphic rocks is considered to be very small (0.1 vol.%). Even assuming a porosity of 1 vol.%, the amount of melt produced would be very small, about 10 wt% of H_2O-undersaturated (4 wt%) melt. This is the main reason why Yardley and Barber (1991) invoked the addition of externally derived H_2O in the genesis of migmatites from Connemara. It must be observed that these works consider the anatexis of high-grade, relatively dehydrated rocks, whereas, in the present discussion, we are modelling the disequilibrium melting of fine-grained metapelites that contain abundant hydrates. There are no precise estimates of the porosity and its evolution in low-grade rocks, but there are data showing that natural porosity can be up to a few per cent in compacted sediments (Szalay 1982). Furthermore, porosity can be enhanced during devolatilization by reaction-induced microcracking, especially in environments characterized by high heating rates (Connolly et al. 1997). Thus, the possibility of achieving transient elevated porosities and of producing high melt fractions also by fluid-present melting cannot be precluded *a priori*, especially in uncommon scenarios such as the present case study. At the same time, the role of fluid infiltration cannot be excluded. However, to account for all the above observations, the external fluid must have been a GCOH mixture at $X_O = 1/3$. Single-pass advection of fluids released by dehydration of underlying graphitic pelites could fullfill these requisites.

Concluding remarks

This work has described an example of disequilibrium behaviour of graphite in anatectic rocks. The presence of only one graphite type (III) that is fully equilibrated at the conditions of partial melting indicates that the xenoliths contain graphites of different origins.

The fate of graphite in the anatexis of the xenoliths of El Joyazo can be modelled as follows. A metapelitic protolith with upper greenschist–facies mineralogy, containing two generations of graphite (types V and VI), is rapidly heated to temperatures in excess of 800 °C. During the subsolidus evolution, fluids released by devolatilization of hydrates consume graphite to produce a GCOH fluid. Simultaneously, graphite undergoes slow and heterogeneous graphitization processes to produce types I, II, and IV. With the onset of partial melting, GCOH fluid depletion induces growth of fluid-deposited, well-ordered type III graphite, with the highest degree of crystallinity observed, typical of granulite-facies conditions.

We envisage the above evolution within a context of disequilibrium, fluid-present melting, accounting for high melt fractions at the estimated temperatures of 850 ± 50 °C. Although this may seem unlikely for most geological scenarios, the chemical and mineralogical constraints imposed by the xenoliths and their potential source rocks demonstrate that this is a feasible mechanism under this peculiar geological setting. Similar behaviour can be expected in rapidly extending crust accompanied by magmatic underplating, and in some contact aureoles. As long as a transient, high porosity is produced this model can be applied to closed-system situations, and obviates any requirement of the infiltration of aqueous fluids.

Acknowledgements This paper benefitted from detailed and constructive reviews by J. Clemens and J. Connolly. We wish to thank E. Burke, J. Dubessy and Gp. Venturelli for discussion on various aspects of this research, P. Lattanzi, J.D. Pasteris and D. Vielzeuf for critical reading of the manuscript, and L. Tauro for patient sample preparation. Financial support was provided by C.N.R..

References

Beny-Bassez C, Rouzaud JN (1985) Characterization of carbonaceous material by correlated electron on optical microscopy and Raman microspectroscopy. Scanning Electron Microsc 1985: 119–132

Bertotti G, ter Voorde M, Cloetingh S, Picotti V (1997) Thermomechanical evolution of the South-Alpine rifted margin (North Italy): constraints on the strength of passive continental margins. Earth Planet Sci Lett 146: 181–193

Burke EAJ, Lustenhower WJ (1987) The application of a multichannel laser Raman microprobe (Microdil 28) to the analysis of fluid inclusions. Chem Geol 61: 11–17

Burnham CW (1967) Hydrothermal fluids at the magmatic stage. In: Barnes HL (ed) Geochemistry of hydrothermal ore deposits, Holt, Rinehart and Winston, New York, pp 34–76

Buseck PR, Huang BJ (1985) Conversion of carbonaceous material to graphite during metamorphism. Geochim Cosmochim Acta 49: 2003–2016

Cesare B (1995) Graphite precipitation within C-O-H fluid inclusions: closed-system chemical and density changes, and thermobarometric implications. Contrib Mineral Petrol 122: 25–33

Cesare B, Salvioli Mariani E, Venturelli G (1997) Crustal anatexis and melt segregation in the restitic xenoliths at El Hoyazo (SE Spain). Mineral Mag 61: 15–27

Clemens JD (1984) Water contents of intermediate to silicic magmas. Lithos 17: 273–287

Clemens JD (1993) Experimental evidence against CO_2-promoted deep crustal melting. Nature 363: 336–338

Clemens JD, Vielzeuf D (1987) Constraints on melting and magma production in the crust. Earth Planet Sci Lett 86: 287–306

Connolly JAD (1995) Phase diagrams for graphitic rocks. Contrib Mineral Petrol 119: 94–116

Connolly JAD, Cesare B (1993) C-O-H-S fluid composition and oxygen fugacity in graphitic metapelites. J Metamorphic Geol 11: 379–388

Connolly JAD, Holness MB, Rubie DC, Rushmer T (1997) Reaction-induced microcracking: an experimental investigation of a mechanism for enhancing anatectic melt extraction. Geology 25: 591–594

De Larouziere FD, Bolze J, Bordet P, Hernandez J, Montenat C, Ott d'Estevou P (1988) The betic segment of the lithospheric Trans-Alboran shear zone during the late Miocene. Tectonophysics 152: 41–52

Eggler DH (1973) Principles of melting of hydrous phases in silicate melt. Carnegie Inst Washington Yearb 72: 491–495

French BM (1964) Graphitization of organic material in a progressively metamorphosed Precambrian iron formation. Science 146: 917–918

Fyfe WS, Price NJ, Thompson AB (1978) Fluids in the Earth's crust. Elsevier, Amsterdam
Grant JA (1985) Phase equilibria in partial melting of pelitic rocks. In: Ashworth JR (ed) Migmatites. Blackie and Son, Glasgow, pp 86–144
Grew ES (1974) Carbonaceous material in some metamorphic rocks of New England and other areas. J Geol 82: 50–73
Hollister VF (1980) Origin of graphite in the Duluth Complex. Econ Geol 75: 764–766
Holloway JR (1976) Fluids in the evolution of granitic magmas: consequences of finite CO_2 solubility. Geol Soc Am Bull 87: 1513–1518
Holloway JR (1987) Igneous fluids. In: Carmichael ISE, Eugster HP (eds) Thermodynamic modelling of geological materials: minerals, fluids and melts. (Reviews in mineralogy, 17) Mineral Soc Am, Washington, DC, pp 211–233
Holloway JR, Pan V, Gudmundsson G (1992) High-pressure fluid-absent melting experiments in the presence of graphite: oxygen fugacity, ferric/ferrous ratio and dissolved CO_2. Eur J Mineral 4: 105–114
Holtz F, Pichavant M, Barbey P, Johannes W (1992) Effects of H_2O on liquidus phase relations in the haplogranite system at 2 and 5 kbar. Am Mineral 77: 1223–1241
Holtz F, Behrens H, Dingwell DB, Johannes W (1995) Water solubility in haplogranitic melts: compositional, pressure and temperature dependence. Am Mineral 80: 94–108
Houseman G, England P (1986) A dynamic model of lithosphere extension and sedimentary basin formation. J Geophys Res 91: 719–729
Itaya T (1981) Carbonaceous material in pelitic schists of the Sanbagawa metamorphic belt in central Shikoku, Japan. Lithos 14: 215–224
Johannes W, Holtz F (1996) Petrogenesis and experimental petrology of granitic rocks. Springer-Verlag, Berlin Heidelberg New York Tokyo
Katz MB (1987) Graphite deposits of Sri Lanka: a consequence of granulite-facies metamorphism. Miner Deposita 22: 18–25
Kerrick DM (1972) Experimental determination of muscovite + quartz stability with $P_{H_2O} < P_{total}$. Am J Sci 272: 946–958
Landis CA (1971) Graphitization of dispersed carbonaceous - material in metamorphic rocks. Contrib Mineral Petrol 30: 34–45
Large DJ, Christy AG, Fallick AE (1994) Poorly crystalline carbonaceous matter in high-grade metasediments: implications for graphitisation and metamorphic fluid composition. Contrib Mineral Petrol 116: 108–116
Le Breton N, Thompson ABT (1988) Fluid-absent (dehydration) melting of biotite in metapelites in the early stages of crustal anatexis. Contrib Mineral Petrol 99: 226–237
Lopez Ruiz J, Rodriguez Badiola E (1980) La region volcanica Neogena del sureste de Espana. Estud Geol 36: 5–63
Michel-Levy C, Lautie A (1981) Microanalysis by Raman spectroscopy of carbon in the Tieschitz chondrite. Nature 292: 321–322
Munskgaard N (1984) High and possible pre-eruptional Rb-Sr isochrons in cordierite-bearing Neogene volcanics from SE Spain. Contrib Mineral Petrol 87: 351–358
Munskgaard N (1985) A non-magmatic origin for compositionally zoned euhedral garnet in silicic Neogene volcanics from SE Spain. Neues Jahrb Mineral Monatsh 2: 73–82
Nemanich RJ, Solin SA (1979) First-and second-order Raman scattering from finite-size crystals of graphite. Phys Rev B 20: 392–401
Oberlin A, Boulmier JL, Villey M (1980) Electron microscopic study of kerogen microtexture: selected criteria for determining the evolution path and evolution stage of kerogens. In: Durand B (ed) Kerogen: insoluble organic matter from sedimentary rocks. Editions Technip, Paris, pp 191–241
Ohmoto H, Kerrick D (1977) Devolatilization equilibria in graphitic systems. Am J Sci 277: 1013–1044
Pasteris JD, Chou I-M (1998) Fluid-deposited graphitic inclusions in quartz: comparison between KTB (German Continental Deep Drilling) core samples and artificially reequilibrated natural inclusions. Geochim Cosmochim Acta 62: 109–122
Pasteris JD, Wopenka B (1991) Raman spectra of graphite as indicators of degree of metamorphism. Can Mineral 29: 1–9
Patiño Douce A, Johnston AD (1991) Phase equilibria and melt productivity in the pelitic system: implications for the origin of peraluminous granitoids. Contrib Mineral Petrol 107: 202–218
Platt JP, England PC (1994) Convective removal of lithosphere beneath mountain belts: thermal and mechanical consequences. Am J Sci 294: 307–336
Platt JP, Soto JI, Comas MC, Leg 16 Shipboard Scientists (1996) Decompression and high-temperature–low-pressure metamorphism in the exhumed floor of an extensional basin, Alboran Sea, western Mediterranean. Geology 24: 447–450
Roedder E (1984) Fluid inclusions. (Reviews in Mineralogy, 12) Mineral Soc Am, Washington, DC
Ross JV, Bustin RM (1990) The role of strain energy in creep graphitization of anthracite. Nature 343: 58–60
Stevens G (1997) Melting, carbonic fluids and water recycling in the deep crust: an example from the Limpopo Belt, South Africa. J Metamorphic Geol 15: 141–154
Szalay A (1982) Possibilities of the reconstruction of basin evolution in the prediction of hydrocarbon prospects. PhD thesis, Hungarian Acad Sci, Budapest
Thompson AB (1982) Dehydration melting of pelitic rocks and the generation of H_2O-undersaturated granitic liquids. Am J Sci 282: 1567–1595
Tsu R, Gonzales H, Hernandez L (1978) Observation of splitting of the E_{2g2} mode and two-phonon spectrum in graphites. Solid State Commun 27: 507–510
Tuinstra F, Koenig JL (1970) Raman spectra of graphite. J Chem Phys 53: 1126–1170
Vielzeuf D, Holloway JR (1988) Experimental determination of the fluid-absent melting relations in the pelitic system: consequences for crustal differentiation. Contrib Mineral Petrol 98: 257–276
Vielzeuf D, Montel JM (1994) Partial melting of metagreywackes. 1. Fluid-absent experiments and phase relationships. Contrib Mineral Petrol 117: 375–393
Wedeking KW, Hayes JM (1983) Carbonization of Precambrian kerogens. In: Bjoroy M (ed) Advances in geochemistry. Wiley, Chichester, pp 546–553.
Wopenka B, Pasteris JD (1993) Structural characterization of kerogens to granulite-facies graphite: applicability of Raman microprobe spectroscopy. Am Mineral 78: 533–557
Wopenka B, Pasteris JD, Bernatowicz TJ, Dunn SR, Valley JW (1988) Si-bearing graphite from Tudor Township, Ontario. EOS Am Geophys Union 69: 65
Yardley BWD, Barber JP (1991) Melting reactions in the Connemara schists: the role of water infiltration in the formation of amphibolite-facies migmatites. Am Mineral 76: 848–856
Yui TF, Huang E, Xu J (1996) Raman spectrum of carbonaceous material: a possible metamorphic grade indicator for low-grade metamorphic rocks. J Metamorphic Geol 14: 115–124
Zeck HP (1968) Anatectic origin and further petrogenesis of almandine-bearing biotite-cordierite-labradorite-dacite with many inclusions of restite and basaltoid material, Cerro de Hoyazo, SE Spain. PhD thesis, Amsterdam
Zeck HP (1970) An erupted migmatite from Cerro de Hoyazo, SE Spain. Contrib Mineral Petrol 26: 225–246
Zeck HP (1996) Betic-Rif orogeny: subduction of Mesozoic Tethys lithosphere under eastward drifting Iberia, slab detachment shortly before 22 Ma, and subsequent uplift and extensional tectonics. Tectonophysics 254: 1–16
Zeck HP, Monie P, Villa IM, Hansen BT (1992) Very high rates of cooling and uplift in the Alpine belt of the Betic Cordilleras, southern Spain. Geology 20: 79–82